Frequency Smearing in Full 3D Interferometry

Pieter van Vugt
University of Twente
Telecommunication Engineering group
P.O. Box 217
7500 AE Enschede, the Netherlands
p.k.a.vanVugt@utwente.nl

Stefan Wijnholds
ASTRON
P.O. Box 2
7990 AA Dwingeloo, the Netherlands
University of Stellenbosch
Electrical and Electronic Engineering
wijnholds@astron.nl

Arjan Meijerink
University of Twente
Telecommunication Engineering group
P.O. Box 217
7500 AE Enschede, the Netherlands
a.meijerink@utwente.nl

Mark Bentum
University of Twente
Telecommunication Engineering group
P.O. Box 217
7500 AE Enschede, the Netherlands
ASTRON
P.O. Box 2
7990 AA Dwingeloo, the Netherlands
m.j.bentum@utwente.nl

Abstract*—Radio astronomy below 30 MHz has never been properly performed because the ionosphere inhibits this on Earth. In order to properly map the sky at these frequencies, the only financially feasible option is to build a radio telescope that comprises many small satellites. Since the observational antennas will be mounted on satellites, rather than on the Earth's surface, the antennas are likely to form a three-dimensional, possibly swarm-like formation. Such a formation will have no preference in direction of observation, which makes filling the full (u, v, w) space an obvious choice, to create a map of the complete celestial sphere at once. Performing interferometry with signals with a larger bandwidth can reduce the amount of visibility data that the satellites need to relay to Earth, assuming correlation is done in space. This can be advantageous if, to avoid man-made radio frequency interference, the satellites are to be deployed in a location far away from Earth. This paper explores the effects that frequency smearing has in this 3D mode of operation, and it is shown to be different from traditional 2D imaging, because the resulting map does not get smeared. Another consequence of correlating with a large bandwidth is bandwidth decorrelation, which is looked into as well. A framework is developed to optimize the sensitivity of the telescope in light of the limited achievable data rate to Earth, in the trade-off between decorrelation and observation bandwidth. Simulation results are presented using the Orbiting Low-Frequency Antennas for Radio Astronomy (OLFAR) concept as a case study.

TABLE OF CONTENTS

1. INTRODUCTION

The last frequency band in radio astronomy that has not yet been properly explored is the one below 30 MHz, in spite of the fact that there are many interesting science cases to do so. Most notably cosmology, where in those frequencies information is expected to be found about the early Universe, from the so-called Dark Ages, and the Epoch of Re-ionization, when the first stars and galaxies were formed [1].

The two main reasons why these frequencies are largely unexplored are the ionosphere and radio-frequency interference (RFI). Radio signals refract in the ionosphere, causing scintillation, and below roughly 10 MHz, depending on the time of day, the signals are even completely blocked. RFI is a problem because the radio spectrum is very crowded below 30 MHz (e.g. AM radio is in that band), and due to sky and ground wave propagation, these signals reach very far. This makes having a radio-quiet zone around the telescope ineffective at these frequencies. An obvious solution to get around these problems is to go into outer space.

A radio observatory on the far side of the moon would be ideal from a scientific point of view, but that is financially impossible. A radio telescope based on conventional satellite technology is described in [2], which uses multiple satellites to form an array. While this is less expensive than building an observatory on the moon, it is still financially prohibitive, given the current state of technology. However, with the rapid development of nano-satellite technology, a satellite-based telescope is quickly becoming financially feasible. Nano-satellites are satellites with a mass of less than 10 kg, and they incorporate many commercially off-the-shelf components, making them relatively inexpensive to design, build and launch. Hence, the most realistic concept of a low-frequency telescope is an array consisting of a constellation of nano-satellites.

One downside of this satellite concept, however, is that the telescope deployment location will likely have to be far away from Earth, to avoid man-made RFI. With the limited electrical power available on nano-satellites, this means that the data rate that can be achieved in the data link to Earth will be severely limited [3]. It would therefore be advantageous to have the satellites perform the correlation in space [4], since the correlations, which are the data needed for imaging, form a much smaller data set than all the individual antenna

978-1-5090-1613-6/17/$31.00

signals. Even then, however, the data rate requirement might still be restrictive if the telescope is deployed far away from Earth. Further reducing the size of the data set might still be necessary.

In a radio telescope observation, the total bandwidth of an observation is commonly divided into many channels, each channel having the same channel bandwidth. Each channel is correlated separately, creating a set of correlations for each channel, to be transmitted to Earth. Hence, the number of channels directly determines the size of the data set that needs to be sent to Earth. One possibility to further reduce the data set is therefore to increase the channel bandwidth, thus reducing the number of channels needed to achieve the observation bandwidth. We will need to asses the consequences for doing so, however, especially since a satellite-based radio telescope has some unique properties that influence these consequences.

A 3D satellite constellation implies that the receiving elements are distributed in a volume, which gives rise to a distribution of baselines in a (u, v, w) space rather than on a (u, v) plane. This is not unusual in Earth-based radio astronomy, except that normally the w component is minimized by design. This is because the goal is to construct a 2D image of, at most, half the celestial sphere, which would be distorted by a large w component in the baselines. The effect of any w component in the baselines is then further minimized by data processing techniques such as polyhedron imaging or joint deconvolution [5].

However, a radio telescope in space, in principle, does not have any direction in which the constellation diameter is smallest or the coverage of the (u, v, w) space is poor. Hence, performing a three-dimensional FFT on the gridded visibility data does not give any specific problems with aliasing due to poor baseline coverage in the w component. This makes keeping the (u, v, w) space fully intact, without attempting to remove one of the dimensions, an interesting proposition, since removing one dimension from the space would mean losing a lot of information.

The consequences of a large channel bandwidth are different for a 3D constellation of antennas than for a 1D or 2D array. It is a well-known fact that when in radio interferometry, the correlation is performed over a wide bandwidth, a point source will show up as a streak in the map. This is called frequency smearing, as the image will be literally smeared [5]. This is one of the main reasons why in radio interferometry, correlation is always performed under narrowband conditions. This holds true for interferometry in one dimension, as well as in two dimensions. However, it will be shown in this paper that in three dimensions, frequency smearing does not occur in the sense that it smears the image. This is because the two-dimensional image that we seek to create (the map) is measured in three dimensions. This leaves one dimension free to contain the frequency information, while in two-dimensional interferometry the frequency information is projected onto the two-dimensional surface together with the map that we seek to create. Hence, frequency smearing is not a problem for imaging with a 3D array.

However, the smearing of the image is not the only consequence of using a large bandwidth. Bandwidth decorrelation is also something that needs to be taken into account, which will decrease the sensitivity of the telescope as the bandwidth per channel increases. This leads to a trade-off between the number of channels, achievable data rate, channel bandwidth and the sensitivity of the telescope. This trade-off will be an important part of the optimization of the overall system design and parameters for the observations.

One of the satellite-based concepts for a radio telescope is currently being developed in the Orbiting Low-Frequency Antennas for Radio Astronomy (OLFAR) project [6, 7]. The OLFAR concept consists of a swarm of 50 or more nano-satellites. All satellites will work together to form a large radio aperture. The swarm will be 100 km in diameter and it will perform interferometry in space from 0.1 to 30 MHz. The deployment location is unknown, at the time of writing. While a Moon orbit is often mentioned, it is not unlikely that another location that is further away from Earth will eventually be chosen [6]. The OLFAR concept is used in this paper as a case study and in simulations, as this concept might benefit from this work when it becomes a reality.

In this paper, we will look into increasing the channel bandwidth to reduce the data rate requirement on the satellite-to-Earth link, as this is likely to be a limiting factor in a radio telescope that is based on nano-satellites. To do this, we will look into the mechanism of frequency smearing, and show that it does not smear the image in 3D imaging, which is confirmed in simulation. By correlating with a larger channel bandwidth, a given frequency range can be represented with a smaller set of correlations, possibly increasing the sensitivity per volume of data. However, when bandwidth decorrelation comes into play, the sensitivity will go down again, creating a trade-off that is explored in this paper.

In the next section, the mechanism of frequency smearing for a 3D constellation of antennas is looked into. In the section after that, the decorrelation effect is presented, and its impact is assessed, resulting in a design trade-off. In Section 4 simulations are presented based on the OLFAR concept, showing the principle of 3D frequency smearing, and conclusions are presented in the last section.

2. FREQUENCY SMEARING

In this section the theory behind frequency smearing is explained, first in one, then in two and finally in three dimensions. First, however, we look into the setup of the interferometer, which explains the bandwidth definitions used in this paper. After that, the one- and two-dimensional cases are explained here for completeness, and, from this, the extension to three dimensions flows most naturally.

Interferometer setup and bandwidths

In radio astronomy, there are various ways to obtain a wideband image. Multiple narrowband images can be combined to create a single wideband intensity map, which is done at the imaging stage. Alternatively, multiple narrowband covariance matrices can be added to obtain a single wideband covariance matrix that can then be used for imaging, afterwards. In this paper however, we consider a wideband correlator. The total observation bandwidth B_{tot} is subdivided into N_{ch} channels, and each channel signal, with bandwidth $B_{\text{ch}} = B_{\text{tot}}/N_{\text{ch}}$, is correlated separately. In this paper we look into the effects of increasing this channel bandwidth, so that the number of channels (and hence the size of the data set to be sent to Earth) can decrease.

Figure 1 illustrates the signal path for a single channel. So in this figure, the channel selection filter subsequent components are implemented N_{ch} times in parallel, each with a

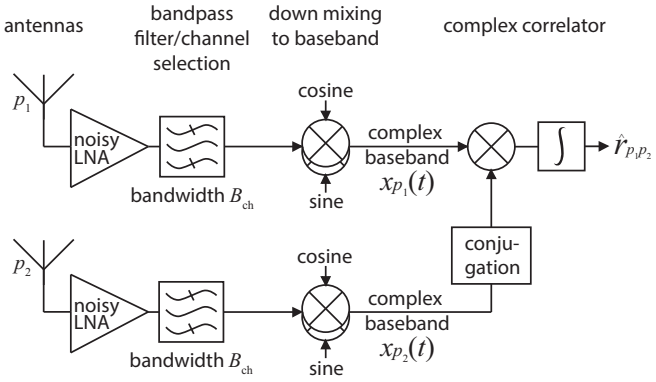

Figure 1. Signal path model for a single frequency channel in an interferometer incorporating two satellites

different center frequency for the channel selection filter.

Frequency smearing in one and two dimensions

In Figure 2, frequency smearing is illustrated for a linear array (that is, the one-dimensional case). In a linear array, a snapshot samples the u-axis, which is normally measured in wavelengths. The distance u is actually the distance between two antennas. The value sampled along this axis is called a visibility. A visibility has a complex value, and its phase corresponds to the phase difference that occurs due to the difference in geometrical delays between two antennas. To visualize this phase, in Figure 2, the real value of the visibility is plotted as a function of u in the lower part of the figure. Note that it is a sinusoid, that looks as if the electrical field of the incoming plane wave has been sampled at the line of the telescope antennas, and is frozen in time. It is frozen in time, because the phase differences between the antennas are time-invariant (assuming the source and antennas are stationary).

As can be seen from Figure 2, the visibilities contain a spatial frequency. In the narrowband, single-frequency case, this spatial frequency only depends on the position of the source, as is illustrated in Figure 2b). In that case, this spatial frequency, after Fourier transform, will provide us with the position of the source. In mathematical terms, for the one-dimensional case, the brightness along the ℓ direction cosine is given by

$$B(\ell) = \mathfrak{F}\{V(u)\} = \mathfrak{F}\left\{e^{j2\pi\ell_s u}\right\} = \int_{-\infty}^{\infty}\left[e^{j2\pi\ell_s u}\right] e^{-j2\pi\ell u} du = \delta(\ell - \ell_s), \quad (1)$$

where u is the baseline length measured in wavelengths, ℓ_s denotes the position of the source, $\mathfrak{F}\{\cdot\}$ denotes the Fourier transform and $\delta(\cdot)$ is the Dirac delta function. The visibility function, $V(u) = e^{j2\pi\ell_s u}$, would in reality of course be sampled by the baselines. We ignore this here for ease of presentation.

Note that ℓ_s is given by

$$\ell_s = \frac{1}{\lambda}(\mathbf{e}_s \bullet \mathbf{e}_u) = \frac{f}{c}(\mathbf{e}_s \bullet \mathbf{e}_u), \quad (2)$$

where $\mathbf{e}_u$ is a unit-vector in the direction of the u-axis, $\mathbf{e}_s$ is a unit vector pointing in the direction of the source, c is the speed of light, and f and λ are the observation radio frequency and wavelength, respectively.

From (2) it can be seen that if, instead of moving the source (changing $\mathbf{e}_s$), we change the radio frequency f at which we measure the source, a similar change in spatial frequency in the visibilities will be observed. This is illustrated in Figure 2b) and 2c). If those two frequencies were correlated at once, the Fourier transform would give two positions for the source. Correlating with a large continuous bandwidth (that is, a large B_{ch}) would then produce a smear instead of a point, after the Fourier transform.

In Figure 3, the planar array case is illustrated. Here, the real parts of the visibilities are represented by a gray-scale value across the (u, v)-plane. Again it looks as if the electric field were sampled at the plane of the baselines and frozen in time. The 2D Fourier transform then gives us the position of the source in (ℓ, m) coordinates, which is a straightforward extention of the one-dimensional case presented in (1) and (2).

We see here something similar, where a different position of the source cannot be distinguished from a different radio

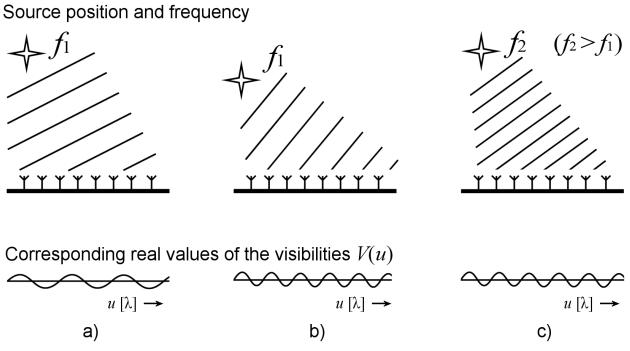

Figure 2. Illustration of a linear array, and its response (real part) to different source positions and observation frequencies

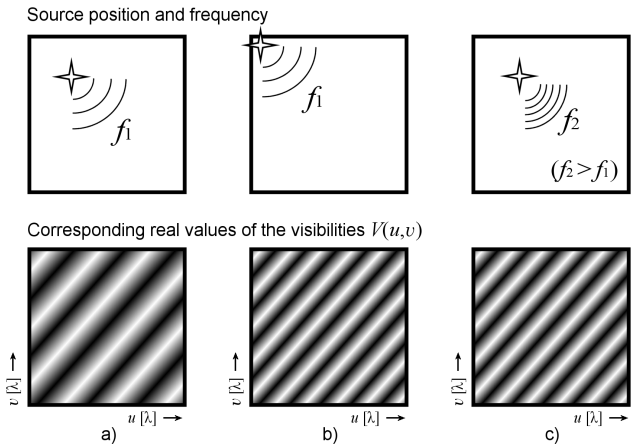

Figure 3. Illustration of the response (real part) of a planar array to different source positions and observation frequencies

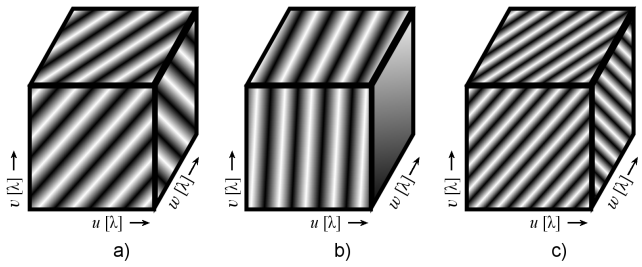

Figure 4. Illustration of the response (real part) of a spatial 3D array to different source positions and observation frequencies

frequency. Hence, after wideband correlation and a two-dimensional Fourier transform, a point source will, again, look like a smear.

Frequency smearing in the three-dimensional case

In the three dimensional case, we are sampling the visibilities across the (u, v, w)-space. Figure 4 illustrates this. (Though only the surface of the (u, v, w)-space is shown, the reader should keep in mind that the whole volume is sampled, not just its surface.)

An incoming plane wave passes though the satellite constellation. Just like in the one- and two-dimensional cases, the resulting visibilities will look as if the electric field were frozen in time and sampled by the baselines, which in this case are distributed in a volume. This frozen electric field has a direction (azimuth and declination) and frequency that are all uniquely visible in the (u, v, w)-space. As can be seen from Figure 4b), changing the direction of the source changes the orientation of the wave in the visibilities. However, it does not look as if the observation frequency were different, like in Figure 4c). This is because the third dimension gives the frequency its own axis to manifest itself along, instead of sharing the axes that represent the position of the source. After a 3D Fourier transform, we find that the sources are positioned on a sphere in the 3D map volume. If the (u, v, w) coordinates of the baselines are measured in wavelengths, as it is commonly done, then the radius of the sphere will be unity under narrow-band conditions. However, if you were to measure them in meters, or if you were to use broadband correlation, we find that the radius of this sphere is dependent on frequency. In other words, the map has three axes: azimuth, declination, and radius, the latter representing radio frequency. Sampling this resulting map along the radial axis, from the origin to a source, gives us the frequency power spectrum of that source.

In Section 4, simulations are presented that illustrate frequency smearing in three dimensions as has been explained in this section.

3. BANDWIDTH DECORRELATION AND SENSITIVITY

Increasing the bandwidth B_{ch} of the signal that is fed to the correlator requires us to look into bandwidth decorrelation. If the bandwidth is too large, the magnitude of $\hat{r}_{p_1p_2}$ decreases with the difference in geometrical delay between antennas p_1 and p_2. This has a negative effect on the sensitivity of the telescope. This is explained in detail in this section, first analytically for a single baseline, then for the telescope as a whole using simulations. After that, the resulting design trade-off is presented.

Decorrelation for a single baseline

Before looking into decorrelation, we need to define the signals that are being correlated more formally. Celestial sources produce signals that can be considered ergodic and stationary. These signals are captured by antennas and, as illustrated in Figure 1, filtered by the channel bandpass filter with bandwidth B_{ch}. We make the assumption here that the Celestial signals have a flat spectrum across the filter bandwidth. After filtering, they are mixed with frequency f_c, down to baseband and represented as a complex baseband signal, $x_p(t)$. This is the signal that gets fed into the correlator.

A correlator is a device that performs the following calculation:

$$\hat{r}_{p_1p_2} = \frac{1}{N}\sum_{n=1}^{N} x_{p_1}(nT)\overline{x_{p_2}(nT)}, \tag{3}$$

where N is the number of samples in an antenna signal for a single snapshot, T is the sample time and the overline denotes conjugation. Since the signals $x_{p_1}(t)$ and $x_{p_2}(t)$ are jointly ergodic, this is an unbiased estimation of the cross correlation function with zero delay,

$$R_{x_{p_1}x_{p_2}}(0) = \mathrm{E}[x_{p_1}(t)\overline{x_{p_2}(t)}], \tag{4}$$

in which $\mathrm{E}[\cdot]$ is the expectancy operator. When N is large, the estimation should be accurate. For the present discussion, we consider a single source and no receiver noise. With these simplifications, both antennas receive the exact same signal, but with a different geometrical delay. Hence, $x_{p_2}(t)$ can be expressed in $x_{p_1}(t)$ as

$$x_{p_2}(t) = x_{p_1}(t - \Delta\tau_{\text{g}})e^{-j2\pi\Delta\tau_{\text{g}}f_c}, \tag{5}$$

where f_c is the center frequency of the observation, $\Delta\tau_{\text{g}}$ is the difference in geometrical delay between antennas p_1 and p_2, and where we assume $p_1 \neq p_2$. Substituting in (4) we get

$$R_{x_{p_1}x_{p_2}}(0) = R_{x_{p_1}}(\Delta\tau_{\text{g}})e^{j2\pi\Delta\tau_{\text{g}}f_c}, \tag{6}$$

in which $R_{x_{p_1}}(\tau) = \mathrm{E}[x_{p_1}(t)\overline{x_{p_1}(t-\tau)}]$ is the autocorrelation function of $x_{p_1}(t)$. We assume that the antenna signal has been filtered by a rectangular channel filter with bandwidth B_{ch}, after which it is down mixed to obtain the complex baseband signal $x_{p_1}(t)$. This passband shape is a realistic assumption, since in an FX-type correlator, the frequency channels are usually created by taking a section out of a wideband signal that has undergone an FFT. The power spectral density of $x_{p_1}(t)$ is then

$$S_{x_{p_1}}(f) = \frac{2P_{x_{p_1}}}{B_{\text{ch}}}\text{rect}\left(\frac{f}{B_{\text{ch}}}\right), \tag{7}$$

where $P_{x_{p_1}}$ is the expected power in $x_{p_1}(t)$, and $\text{rect}(\cdot)$ is the rectangular function given by

$$\text{rect}(x) = \begin{cases} 1, & |x| \leq 1/2, \\ 0, & |x| > 1/2. \end{cases} \tag{8}$$

Since $x_{p_1}(t)$ is a stationary process, the Wiener-Khinchin theorem tells us that the autocorrelation of $x_{p_1}(t)$ is

$$R_{x_{p_1}}(\Delta\tau_{\text{g}}) = 2P_{x_{p_1}}\,\text{sinc}\left(\pi B_{\text{ch}}\Delta\tau_{\text{g}}\right), \tag{9}$$

where the sinc function is given by $\text{sinc}(x) = \sin(x)/x$. Substituting in (6) we have

$$R_{x_{p_1}x_{p_2}}(0) = 2P_{x_{p_1}}\{e^{j2\pi\Delta\tau_g f_c}\}\text{sinc}\left(\pi B_{\text{ch}}\Delta\tau_g\right). \quad (10)$$

In this equation we find the expectation of the narrowband response of the correllator (where $B_{\text{ch}}\Delta\tau_g \approx 0$),

$$R_{x_{p_1}x_{p_2}}(0)\Big|_{\text{narrowband}} \approx 2P_{x_{p_1}}e^{j2\pi\Delta\tau_g f_c}, \quad (11)$$

times the decorrelation factor

$$D(B_{\text{ch}}, \Delta\tau_g) = \text{sinc}(\pi B_{\text{ch}}\Delta\tau_g). \quad (12)$$

Note that this factor depends on the baseline as well as on the position of the source, but is independent of f_c. And while the decorrelation factor is real, it is not necessarily positive. Another thing to note, is that the sinc function is a direct result of the band pass shape of the channel filter. Changing the shape of this passband will hence also change the form of the decorrelation factor. Changing the passband shape might be a way to optimize the decorrelation factor so that its effect on the sensitivity of the instrument as a whole decreases. However, this is not further considered here.

Decorrelation for the whole telescope

Now that we have derived an expression for decorrelation for a single baseline, we need to investigate what this will mean for the telescope as a whole, as it contains a large number of different baselines. Hence we want to see what the average decorrelation is, which we denote by D_{av}

While it might be possible to derive an analytical expression for D_{av}, such an expression would be complicated and cumbersome. Furthermore, its form would be heavily dependent on the assumptions made for the satellite distribution and the choice of pass-band filter shape used to make the frequency channels. It is, however, quite straightforward to get an accurate simulated estimate, and when the deployment location and satellite trajectories are known, simulation is likely the only way to obtain the D_{av} curve as a function of B_{ch}.

For this reason, Monte-Carlo (MC) simulations have been performed, using the OLFAR specifications as a basis. This means that 50 satellites are assumed in a swarm-like formation. The distribution of the satellites is assumed Gaussian, in the sense that their Cartesian coordinates are chosen independently random with a Gaussian probability distribution. This distribution was chosen for its mathematical tractability, and because it results in a desirable coverage of the (u, v, w)-space. When an actual satellite-based radio telescope is deployed, its constellation will likely not be Gaussian distributed. However, such a distribution would be approximated as closely as the orbits at the deployment location would allow. The diameter of the OLFAR swarm is approximately 100 km, and for this reason the standard deviation of the satellite coordinates σ_{P} is chosen to be 25 km, which is used in this section as an example when appropriate.

For every MC iteration, a new swarm with new satellite positions was randomly generated. Three sources were positioned perpendicularly with respect to each other along the primary axes. This way, each source has its own collection of $\Delta\tau_g$ values, and these three collections are mutually independent. The value of $\Delta\tau_g$ depends on the difference in geometrical delay due to two satellite positions. The distribution of $\Delta\tau_g$

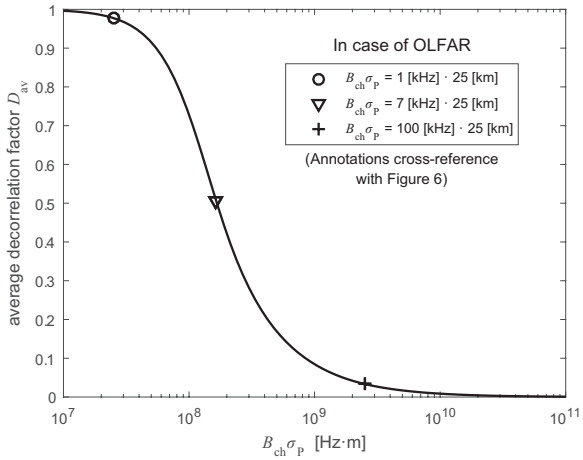

Figure 5. Estimated average decorrelation factor vs. bandwidth times the standard deviation of the satellite distribution, $B_{\text{ch}}\sigma_{\text{P}}$

is therefore also Gaussian, where the variance is given by

$$\sigma^2_{\Delta\tau_g} = \frac{2\sigma^2_{\text{P}}}{c^2}. \quad (13)$$

This means that the probability distribution of (12) scales horizontally with σ_{P}. Hence we can calculate the average decorrelation factor D_{av} as a function of the product $B_{\text{ch}}\sigma_{\text{P}}$. In this way it is more clearly shown how the average decorrelation factor is affected by both the channel bandwidth and the dimensions of the satellite constellation. So in the simulation, the decorrelation factors for all source-baseline combinations were calculated as a function of $B_{\text{ch}}\sigma_{\text{P}}$, and the resulting curves were averaged. These curves were also averaged across all MC iterations, and the final curve is presented in Figure 5. In this figure, some values are annotated for the specific case of OLFAR.

This figure can be further interpreted if we first look at the probability density function (PDF) of the decorrelation factor. This PDF was estimated for several bandwidths in the same simulation and the result is presented in Figure 6.

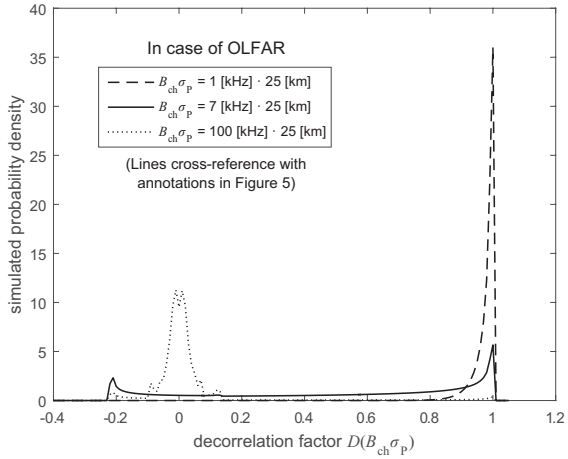

Figure 6. Estimated PDF of the decorrelation factor for various $B_{\text{ch}}\sigma_{\text{P}}$

It can be seen that the values of the decorrelation factors of the individual source-baseline combinations have a tendency to be grouped either around one or zero, with few in between. So by approximation, we can say that either a baseline is sensitive to a source, or it is insensitive to a source due to decorrelation. Therefore, the value of $D_{\text{av}}(B_{\text{ch}}\sigma_{\text{P}})$ in Figure 5 can be interpreted as the average fraction of baselines that are sensitive to any source. For a value of $B_{\text{ch}}\sigma_{\text{P}}$ of $1.6 \cdot 10^8$ ($\approx$ 7[kHz] $\cdot$ 25[km] annotation in the figures), about half of the baselines are sensitive and half of the baselines are not. Of course, it must be noted that the baselines that are insensitive for a source in one direction will still be sensitive for sources in different directions.

Another interesting way to look at the decorrelation, is to see what effect it has on the spatial frequencies in the sky that we want to image. Take the component of a baseline, projected onto a surface perpendicular the direction of arrival (DOA) of a source signal. We will call this the perpendicular baseline component. When this perpendicular component is short, a low spatial frequency is sampled. Such low frequencies are prominent in extended sources, such as the Milky Way. When the perpendicular component is long, a high spatial frequency is sampled. Such high frequencies are important for imaging small features, such as point sources.

For a fixed channel bandwidth, when looking at a single baseline with a certain length, its orientation with respect to the DOA determines both the decorrelation and the spatial frequency it samples. In this case, these quantities are directly related. A high spatial frequency (long perpendicular component) means a high decorrelation factor, and vice versa.

However, in a constellation with many different baseline lengths and orientations, it becomes relevant to look at this problem from a statistical point of view. So we want to look into whether baselines with a large perpendicular component are, on average, affected more by the decorrelation factors compared to baselines with a smaller perpendicular component. Or in other words, if the high spatial frequencies are affected more by decorrelation than the lower spatial frequencies.

However, with the Cartesian coordinates of the satellites chosen independently with a Gaussian probability density, all spatial frequencies would be affected the same amount. This is because the perpendicular baseline components and the baseline components in the DOA, which determine the geometrical delays, are not correlated. However this is a result of the very specific assumption we made about the satellite distribution. If you look at a slightly different distribution of satellites, the result will be different. The high spatial frequencies might well be affected significantly more than the low spatial frequencies.

While this is a question to look into when designing a radio telescope based on satellites, the result of this question is very dependent on the exact distribution of the satellites. Hence, no meaningful simulation or rule of thumb can be presented about it, without more knowledge about the actual satellite distribution.

Design for Optimal Sensitivity

In the previous subsection, we looked into the average decorrelation factor for the radio telescope constellation as a whole. The next step is to see what this means for the sensitivity of the telescope. The sensitivity of a telescope is defined as the 1σ detection limit, which is the lowest flux density from a source that the instrument can detect with an SNR of 1. This limit is given by [5, 8]

$$\Delta S = \frac{2kT_{\text{sys}}}{A_{\text{eff}}\sqrt{B_{\text{tot}}\mathcal{T}_{\text{int}}}}, \tag{14}$$

where B_{tot} is the total observation bandwidth, A_{eff} is the total effective antenna area of the telescope, $\mathcal{T}_{\text{int}}$ is the integration time, T_{sys} is the equivalent system temperature and k is the Boltzmann constant. This formula is valid under the narrowband assumption, as decorrelation is not taken into account. Note that the smaller ΔS, the more sensitive the instrument. The signal-to-noise ratio of a measurement of a certain source follows from

$$\text{SNR} = \frac{S_{\text{s}}}{\Delta S} = \frac{S_{\text{s}}A_{\text{eff}}}{2kT_{\text{sys}}}\sqrt{B_{\text{tot}}\mathcal{T}_{\text{int}}}, \tag{15}$$

in which S_{s} is the flux density of the source. Now for our analysis, S_{s}, $\mathcal{T}_{\text{int}}$ and $(A_{\text{eff}}/T_{\text{sys}})$ are constants, as they are determined by other (system) parameters. The SNR directly depends on the total effective collecting area A_{eff}, which scales with the number of satellites P. The number of baselines, on the other hand, scales with P^2. Hence, incorporating $D_{\text{av}}(B_{\text{ch}}\sigma_{\text{P}})$ into (15) gives us

$$\text{SNR} = \frac{S_{\text{s}}}{\Delta S} = \frac{S_{\text{s}}A_{\text{eff}}}{2kT_{\text{sys}}}\sqrt{B_{\text{tot}}\mathcal{T}_{\text{int}}D_{\text{av}}(B_{\text{ch}}\sigma_{\text{P}})}. \tag{16}$$

Every channel, assuming a constant integration time, generates a certain volume of data. The number of channels that need to be transmitted from the satellites to Earth is defined as $N_{\text{ch}} = B_{\text{tot}}/B_{\text{ch}}$. We want to achieve an SNR as high as possible with as little data as possible. So we look at the sensitivity per data volume, which is proportional to the number of channels, and is given by

$$\frac{\text{SNR}}{N_{\text{ch}}} = \frac{1}{N_{\text{ch}}}\frac{S_{\text{s}}A_{\text{eff}}}{2kT_{\text{sys}}}\sqrt{B_{\text{tot}}\mathcal{T}_{\text{int}}D_{\text{av}}(B_{\text{ch}}\sigma_{\text{P}})}. \tag{17}$$

This equation allows us to optimize the sensitivity per data volume by cleverly choosing B_{ch}, B_{tot} and N_{ch}, while taking into account the limitations of the system, such as a maximum value for N_{ch} due to the satellite-to-Earth link or the maximum of B_{tot} due to the receiver topology.

To illustrate such an optimization, we look at the example of OLFAR. We assume the limiting factor is the achievable data rate towards Earth, so we calculated SNR/N_{ch} as a function of B_{ch} for several fixed values of N_{ch}. We assume $S_{\text{s}}A_{\text{eff}}/(2kT_{\text{sys}}) = 1$ and $\mathcal{T}_{\text{int}} = 1$ without loss of generality, since the curve only scales vertically with these quantities.

Figure 7 shows the resulting curves. The current design for OLFAR has an instantaneous bandwidth of $B_{\text{tot}} = 1$ MHz, which is subdivided into $N_{\text{ch}} = 1000$ channels, meaning $B_{\text{ch}} = 1$ kHz. Because B_{tot} is limited by the receiver design, in Figure 7, the lines where $B_{\text{tot}} > 1$ MHz are dashed, and the lines end at $B_{\text{tot}} = 30$ MHz because at that point the whole frequency band of interest is captured in a single observation.

From Figure 7 it can be seen that increasing the channel bandwidth B_{ch} has a positive influence on the sensitivity of the instrument per data volume. However for large values of B_{ch}, the effect of the increasing bandwidth is canceled by the decreasing decorrelation factor, leading to the horizontal asymptotes. As a result, the value of B_{ch} can be

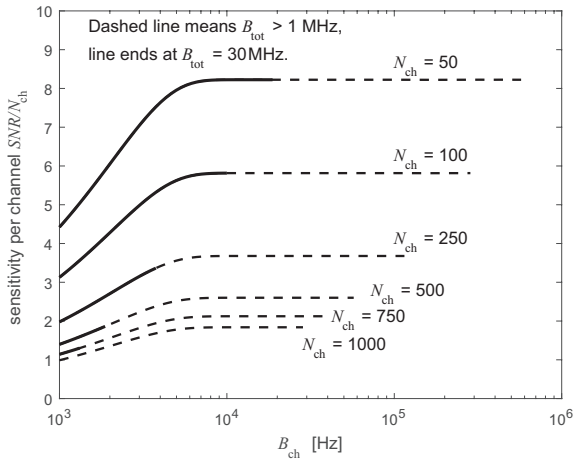

Figure 7. **Sensitivity per channel** $\mathrm{SNR}/N_{\mathrm{ch}}$ **vs. channel bandwidth** B_{ch} **for several numbers of channels** N_{ch}**, for the case of OLFAR**

made arbitrarily large without degrading the sensitivity due to decorrelation.

Although the results shown here are based on simulations with very specific assumptions on the positions of the satellites (Gaussian distributed) and the transfer functions of the channel filters (rectangular-shaped), it can easily be shown from analytical considerations that these asymptotes will remain when these assumptions are generalized. Nevertheless, the actual asymptotic value of the SNR per channel might well depend on these assumptions. The same applies to the value of the channel bandwidth B_{ch} for which the SNR per channel starts to approach this asymptotic value, possibly leading to a value that exceeds 30 MHz.

Table 1. **Simulation conditions**

Parameter	**Value**	**Unit**
Number of satellites	50 or 125*	
Antennas per satellite	3	
Channel center frequency	100	kHz
Channel Frequency band	75 – 125 or	kHz
	85 – 115*	kHz
Channel bandwidth	50% or 30%*	
Swarm diameter (approx.)	100	km
Satellite distribution	Gaussian**	
Integration time	1	seconds
Receiver noise power	$1.0 \cdot 10^4$	relative ***
Source powers (received)	0.5 – 1	relative ***
Number of sources	1 or 5*	

* mentioned in text
** details in subsection *Decorrelation for the whole telescope*
*** to the highest received source power

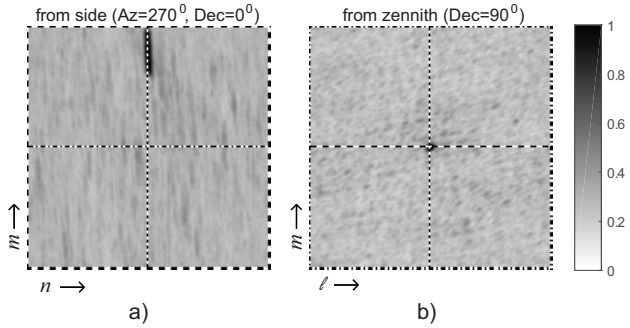

Figure 8. **Image space resulting from a simulated wideband single-channel observation of a single point source in zenith emitting white noise, shown from two angles**

4. SIMULATIONS

In this section, simulation results are shown that verify the findings presented in Section 2, namely that frequency smearing causes no problems for imaging with a 3D array. The OLFAR simulator that was used for developing the calibration routine in [9, 10] has been adapted to take wideband snapshots, where a single channel is simulated. The properties of this simulation are listed in Table 1.

The visibilities from the simulation were gridded by placing them on the nearest grid point in the (u, v, w)-space, after which a 3D FFT was performed. The result of the 3D FFT is an image space in (ℓ, m, n)-coordinates that contains the map. The intensity in this map has been normalized with respect to the strongest source, because the simulator was not designed to provide an insightful scale. In spite of the rather crude imaging technique however, the images show a clear result.

An observation was simulated with a single source positioned in zenith, using 50 satellites and a 50% relative bandwidth. The image in Figure 8 shows the resulting image space from two sides. Figure 8a) clearly shows the frequency smearing when we are looking at the resulting volume map from the side (0 degrees declination). However when we look at the image space from the direction of the source, as in Figure 8b), we see a single dot marking the position of the source. Hence, the position of the source is well defined and a resulting 2D map would not be smeared.

In Section 2, it was claimed that the frequency manifests itself along the radial axis, so we expect to see the spectrum of the source on this axis. To test this, in the next simulation, the source in zenith is not transmitting white noise, but has a spectrum as shown in Figure 9. This spectrum was chosen so that we would be able to distinguish the low frequencies from the high frequencies. The resulting map is shown in Figure 10.

When we look at this map, we observe two clear dots with different intensity along the radial axis, as was expected from theory. From the different intensity of the dots, We clearly recognize the power spectrum of the source, where 0 Hz is at the origin, and the maximum frequency is furthest away from the origin.

To illustrate that the theory does not break down when the sky model is more than a single point source, a simulation with

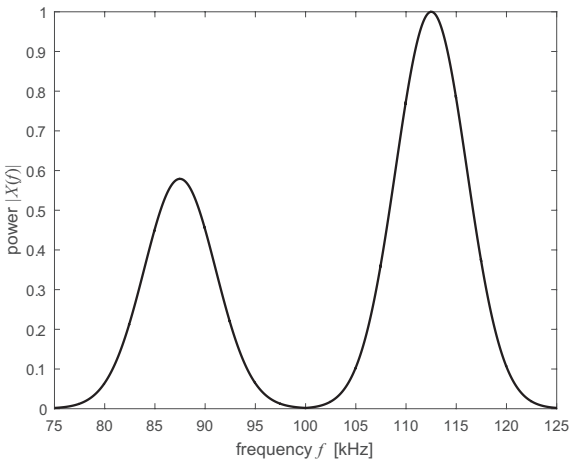

Figure 9. Power spectral density of the simulated source imaged in Figure 10, in relative units

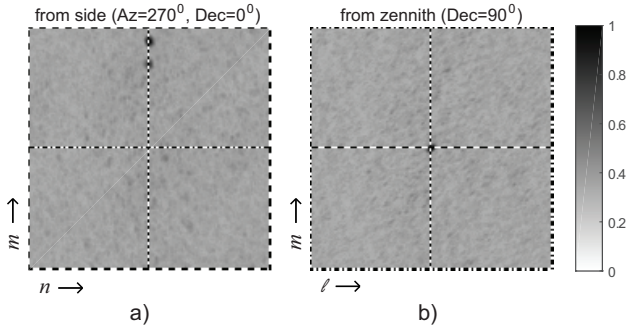

Figure 10. Image space resulting from a simulated wideband single-channel observation of a single point source emitting colored noise, shown from two angles

five sources was performed as well. This simulation used 125 satellites instead of 50 and with a lower relative bandwidth of 30%, to cope with the more complex sky model. Figure 11 shows the resulting image volume. Each source is clearly seen as a smear along the radial axis. In Figure 12, the 2D map is shown from this simulation. Each pixel of this map is the result of an integration along the radius of the image space, i.e. along the frequency axis, and represents the total power from each source within the channel bandwidth. As can be seen, the sources are not smeared in the resulting map.

5. CONCLUSIONS

A nano-satellite-based 3D radio interferometry array was considered. Reducing the data volume that has to be sent to Earth can be accomplished by increasing the channel bandwidth. This way, fewer frequency channels need to be sent to Earth while still achieving the total observation bandwidth. Through theory and simulation, it is shown that frequency smearing, which occurs if the channel bandwidth is high, is not a problem for imaging when the visibilities in the full (u, v, w)-space are processed by a 3D FFT. However, bandwidth decorrelation does occur if the bandwidth in the correlators is large. Together with other system parameters and restrictions, this leads to a possible trade-off, because

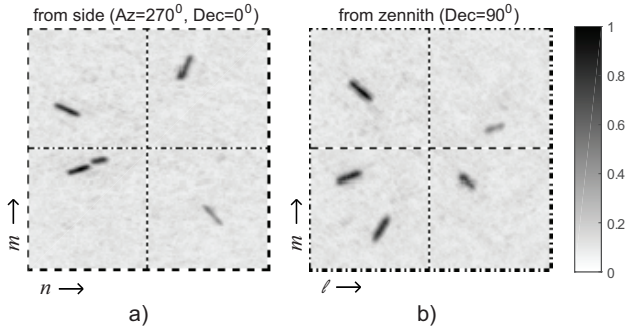

Figure 11. Image space resulting from a simulated wideband single-channel observation of five point sources, shown from two angles

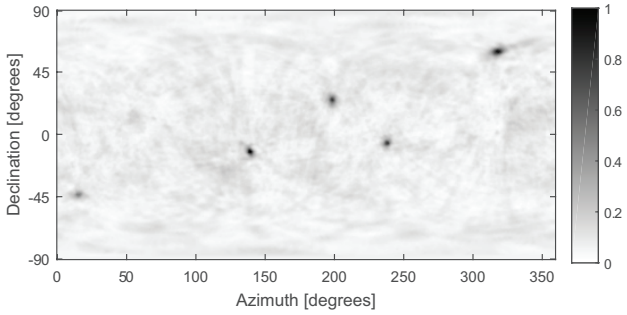

Figure 12. 2D projected map of the full simulated sky where each pixel is the result of integration along the radius of the image space shown in Figure 11

increasing the total bandwidth increases the sensitivity of the instrument, while bandwidth decorrelation will decrease it again if it becomes too severe. A framework is presented that can be used to find the optimum in sensitivity, given the restraint in number of channels, using analytic derivations and simulations where appropriate. The mechanisms at play are presented and it is shown how to find the optimum in this trade-off once the deployment location and the exact orbits of the satellites are known.

ACKNOWLEDGMENTS

This work is part of the DCIS (Data Collecting Colonies in Space) project, which is supported by NanoNextNL, a micro and nanotechnology consortium of the Government of the Netherlands and 130 partners.

REFERENCES

[1] S. Jester and H. Falcke, "Science with a lunar low-frequency array: From the dark ages of the universe to nearby exoplanets," *New Astronomy Reviews*, vol. 53, no. 1-2, 2009.

[2] N. Saks, A.-J. Boonstra, R. T. Rajan, M. Bentum, F. Beliën, and K. van 't Klooster, "DARIS, a fleet of passive formation flying small satellites for low frequency radio astronomy," in *Small Satellite Systems and Services - The 4S Symposium*. ESA en CNES, June 2010.

[3] A. Budianu, A. Meijerink, and M. J. Bentum, "Swarm to Earth communication in OLFAR," in *Proceedings of the 64th IAC International Astronautical Congress*, Beijing, China, September 2013.

[4] R. Rajan, M. Bentum, A. Gunst, and A. Boonstra, "Distributed correlators for interferometry in space," in *IEEE Aerospace Conference*, March 2013.

[5] G. B. Taylor, C. L. Carilli, and R. A. Perley, Eds., *Synthesis Imaging in Radio Astronomy II*, ser. Astronomical Society of the Pacific Conference Series, vol. 180, 1999.

[6] M. Bentum, C. Verhoeven, A. Boonstra, E. Gill, and A. van der Veen, "A novel astronomical application for formation flying small satellites," in *60th International Astronautical Congress*, Daejeon, October 2009.

[7] R. Rajan, S. Engelen, M. Bentum, and C. Verhoeven, "Orbiting low frequency array for radio astronomy," in *IEEE Aerospace Conference*, March 2011.

[8] A. Thompson, J. Moran, and G. Swenson, *Interferometry and Synthesis in Radio Astronomy*. Wiley, 2008. [Online]. Available: https://books.google.nl/books?id=S99Z7kNBYzAC

[9] P. van Vugt, A. Budianu, A. Meijerink, and M. Bentum, "Calibration approach of the OLFAR space based radio telescope," in *Proceedings of the 65th International Astronautical Congress*, Toronto, Canada, September 2014.

[10] P. van Vugt, A. Meijerink, and M. Bentum, "Calibration of the OLFAR space-based radio telescope using an alternating least squares approach," in *2016 IEEE Aerospace Conference*, March 2016.

BIOGRAPHY

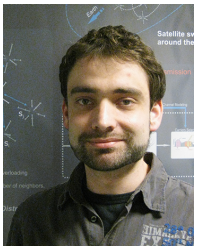

Pieter K. A. van Vugt *was born in Nijmegen, The Netherlands, in August 1983. He received the B.Sc. and M.Sc. degrees in Electrical Engineering from the University of Twente, Enschede, The Netherlands, in April 2010 and July 2013, respectively. He is currently working towards the Ph.D. degree at the same university. The topic of his research is the calibration of the space-based radio telescope OLFAR.*

Stefan J. Wijnholds *(S'06-M'10-SM'12) was born in The Netherlands in 1978. He received the M.Sc. degree in astronomy and the M.Eng. degree in Applied Physics (both cum laude) from the University of Groningen, the Netherlands, in 2003, and the Ph.D. degree (cum laude) from Delft University of Technology, Delft, The Netherlands, in 2010. After his graduation in 2003, he joined the R&D Department of ASTRON, the Netherlands Institute for Radio Astronomy, in Dwingeloo, The Netherlands, where he works with the system design and integration group on the development of the next generation of radio telescopes. From 2006 to 2010, he was also affiliated with the Delft University of Technology, Delft, The Netherlands, and in 2016, he was appointed as Extraordinary Associate Professor at the University of Stellenbosch in South Africa. His research interests lie in the area of array signal processing, specifically calibration and imaging, and system design of the next generation of radio telescopes.*
He is a Senior Member of IEEE. He is the Early Career Representative (ECR) for URSI Commission J (Radio Astronomy) and chair of the ECR Committee. He is also associate editor for the Radio Science Bulletin and the journal Radio Science and is a regular reviewer for various conferences and journals. He is a member of the scientific organizing committee of the SKA Calibration & Imaging Workshop series.

Arjan Meijerink *(S'00-M'06-SM'11) received the M.Sc. and Ph.D. degrees in Electrical Engineering (both with honors) from the University of Twente, Enschede, the Netherlands, in 2001 and 2005, respectively. In 2000 he was a Trainee at Ericsson Business Mobile Networks in Enschede. From 2001 he has been working at the University of Twente, initially as a Research Assistant, and from 2005 as a Postdoctoral Researcher. Since 2007 he has been an Assistant Professor in short range radio. In 2009 he was a Visiting Lecturer at the Queen's University, Belfast, U.K., and in 2010 he was a Visiting Scholar at the University of Southern California, Los Angeles, U.S.A. Dr. Meijerink has published more than 50 papers in international journals, conferences and symposia. He is a member of IEEE and URSI, and has reviewed for various journals, conferences and symposia. Currently he is a member of the Executive Committee of the IEEE Benelux Joint Chapter on Communications and Vehicular Technology.*

Mark J. Bentum *(S'92-M'95-SM'09) was born in Smilde, the Netherlands, in 1967. He received the M.Sc. degree in Electrical Engineering (with honors) from the University of Twente, Enschede, the Netherlands, in August 1991. In December 1995 he received the Ph.D. degree for his thesis "Interactive Visualization of Volume Data", also from the University of Twente. From December 1995 to June 1996 he was a Research Assistant at the University of Twente in the field of signal processing for mobile telecommunications and medical data processing. In June 1996 he joined the Netherlands Foundation for Research in Astronomy (ASTRON). He was in various positions at ASTRON. In 2005 he was involved in the eSMA project in Hawaii to correlate the Dutch JCMT mm-telescope with the Submillimeter Array (SMA) of Harvard University. From 2005 to 2008 he was responsible for the construction of the first software radio telescope in the world, LOFAR (Low Frequency Array). In 2008 he became an Associate Professor in the Telecommunication Engineering Group at the University of Twente. He is now involved with research and education in mobile radio communications. His current research interests are short-range radio communications, novel receiver technologies (for instance in the field of radio astronomy), channel modeling, interference mitigation and sensor networks. Dr. Bentum is a Senior Member of the IEEE, Chair of the Dutch URSI committee, initiator and chair of the IEEE Benelux AES/GRSS Chapter, member of the Dutch Royal Institute of Engineers KIVI NIRIA and the Dutch Pattern Recognition Society, and has acted as a reviewer for various conferences and journals.*